Energy and power characteristics of nanocatalyzed Belousov-Zhabotinsky reactions via bifurcation analyses

Vandana Rajput and Pratyush Dayal *

Polymer Engineering Research Laboratory (PERL), Department of Chemical Engineering, Indian Institute of Technology Gandhinagar, Gujarat-382055, India

(Received 2 September 2023; accepted 22 November 2023; published 21 December 2023)

Active stimuli-responsive materials, intrinsically powered by chemical reactions, have immense capabilities that can be harnessed for designing synthetic systems for a variety of biomimetic applications. It goes without saying that the key aspect involved in the designing of such systems is to accurately estimate the amount of energy and power available for transduction through various mechanisms. Belousov-Zhabotinsky (BZ) reactions are dynamical systems, which exhibit self-sustained nonlinear chemical oscillations, as their catalyst undergoes periodic redox cycles in the presence of reagents. The unique feature of BZ reaction based active systems is that they can continuously perform mechanical work by transducing energy from sustained chemical oscillations. The objective of our work is to use bifurcation analyses to identify oscillatory regimes and quantify energy-power characteristics of the BZ reaction based on nanocatalyst activity and BZ reaction formulations. Our approach involves not only the computation of higher order Lyapunov and frequency coefficients but also Hamiltonian functions, through normal form reduction of the kinetic model of the BZ reaction. Ultimately, using these calculations, we determine amplitude, frequency, and energy-power densities, as a function of the nanocatalysts' activity and BZ formulations. As normal form representations are applicable to any dynamical system, we believe that our framework can be extended to other self-sustained active systems, including systems based on stimuli-responsive materials.

DOI: 10.1103/PhysRevE.108.064211

I. INTRODUCTION

Synthetic soft materials [1–5] that can harness energy via chemomechanical transduction [1,2,6–13] have provided significant impetus in the field of active matter design. These active soft materials have been used for designing a variety of artificial multifunctional systems that have the ability to mimic biological functionalities [14–16]. For instance, active polymer gels have been known to produce mechanical deformations based on the chemical stimuli that they are subjected to [17–19]. Likewise, active droplets, fueled by chemical reactions, generate asymmetric Marangoni flows and exhibit directed spontaneous locomotion [20–22]. It goes without saying that the mechanical work produced by these systems is a direct consequence of their inherent capability to effectively utilize the energy emanating from chemical reactions. In this context, Belousov-Zhabotinsky (BZ) reaction [23–28] based active systems are unique as they transduce energy, from sustained chemical oscillations, to produce continuous mechanical work [6–10,21,22]. The objective of our work is to establish energy and power characteristics of the nanocatalyzed BZ reaction, of different formulations, using nonlinear bifurcation analyses. As BZ reaction based active systems are essentially nonlinear dynamical systems that operate far from equilibrium, the approach presented here can be harnessed to probe innate energy and power characteristics of other active systems as well. Typical applications include autonomous nano- and micromotors [29–31], artificial microswimmers for delivering nanoscopic cargos [32,33], drug delivery [33,34], and chemical sensors [35,36], to name a few.

The BZ reaction is a nonlinear chemical oscillator wherein the catalyst undergoes sustained redox cycles in the presence of reagents [23–28]. More often than not, these chemical oscillations manifest as the periodic color change of the BZ solution. Traditionally, solution-based metal ions have been used to catalyze the BZ reaction [37–39], however, recently it has been demonstrated that the use of nanocatalysts [40–42] enhances the dynamics of the BZ reaction in a very significant manner. In particular, the use of nanoparticle (NP) decorated graphene-based nanosheets as a catalyst [40,41] has resulted in enhanced dynamics of chemical oscillations in the BZ reaction system. Similar observations have been made when bare ceria nanosheets [42] are used to catalyze the BZ reaction. In essence, the use of high performance nanocatalysts has opened up new avenues in the design of BZ reaction based active systems. For instance, through modeling, simulation, and experimental investigations, it has been demonstrated that nanocatalyzed BZ droplets exhibit 1.75 times higher velocities compared to their traditional counterparts [21]. Similar arguments can be made regarding BZ gels [6–8,10] that exhibit great potential to be used as mass transport devices, artificial pacemakers, cilia, sensors, actuators, etc. [6,8,10]. Thus, apart from dynamical characteristics such as amplitude and frequency, it becomes imperative to determine the amount of energy from BZ reactions that can be harnessed through

*pdayal@iitgn.ac.in

various mechanisms including chemomechanical transduction. The quantification of energy and power attributes of the BZ reaction, therefore, not only facilitates the design of self-sustained dynamical systems but also plays a key role in formulating strategies for finer control and regulation of their response. Our work focuses on utilizing bifurcation analyses to describe the dynamics of nanocatalyzed BZ reactions, quantify energy of BZ oscillations, and identify conditions under which this energy can be utilized to power other external systems. Furthermore, we also explore energy and power characteristics for various nanocatalysts and changes in the BZ recipe.

Mathematically, it has been known that the chemical oscillations in the BZ reaction are realized when the steady state loses its stability through Hopf bifurcation (HB) [43]. As a matter of fact, many different types of bifurcations [23,44–46] have been identified in the BZ reaction system that use traditional solution-based catalysts. In most of the cases, the Oregonator model [47,48], which is the mathematical representation of the Field-Koros-Noyes (FKN) mechanism [49], has been used for bifurcation analyses, however, the usage of other models [45] is not uncommon. Recently, the nanocatalysts' activity has been incorporated into the Oregonator model [42,50] by identifying key steps in the FKN mechanism, and the oscillatory dynamics of various nanocatalyzed BZ reactions have been determined [50]. On the energy front, it has already been established that the sustained chemical oscillations in the BZ reaction take place at the expense of continuous decrease in the Gibbs free energy [51]. To the best of our knowledge, however, the determination of energy and power attributes of the BZ reaction has largely been missing, although the Gibbs energy of other chemically oscillating systems has been determined both experimentally [52] and numerically [53]. In our approach, we calculate energy and power densities using Hamiltonian functions for different nanocatalysts and BZ formulations, wherein the Oregonator model has been employed to account for changes in the BZ recipe and nanocatalyst activity. As the energy of chemical oscillations is primarily the Gibbs free energy of the system calculated from the redox potentials [52], the use of Hamiltonian functions enables us to calculate the total chemical energy stored in BZ oscillations directly from its amplitude-frequency characteristics. These dynamical attributes of the BZ reaction, on the other hand, can be determined experimentally from the redox potentials [52], using the chronopotentiometry (CP) [42] and image processing (IMP) techniques [40–42].

It is important to note that the energy and power density calculations from chemical oscillations are also dependent upon whether the BZ reaction system is conservative or nonconservative. When the BZ reaction operates at the limit cycle (LC) it is conservative [54], as all the inherent chemical energy is utilized for oscillations and no energy is available for powering external systems. The BZ reaction, however, becomes nonconservative [54] when it operates between steady state and the LC and thus can be harnessed to continuously transduce chemical energy into mechanical work. For instance, polymer hydrogels internally powered by the BZ reaction are known to produce sustained mechanical oscillations by chemomechanical transduction. Thus, by comparing the energies of chemical oscillations for BZ reactions with mechanical oscillations for BZ-powered hydrogels, the efficiency of chemomechanical transduction can be established. Here, however, we have focused on developing the methodology to facilitate these calculations and the computation of energy-power densities for other systems powered by the BZ reaction are beyond the scope of this paper. As any dynamical system can be recast into its normal form, the distinct advantage of using our methodology for performing energy-power calculations is that it can be extended to other dynamical systems, active or inactive.

The rest of the paper is organized into different sections and subsections. We start with the Methodology (Sec. II) with the description of the Oregonator model and introduce dimensionless parameters and variables required for bifurcation analyses (Sec. II A). Subsequently, we compute the steady states, their stability, and higher order bifurcations using the normal form of the model equations (Sec. II B). Ultimately, we develop both conservative and nonconservative Hamiltonian functions (Sec. II C) for the calculation of energy and power densities. In Results and Discussions (Sec. III), we report our major outcomes and discuss their implications in the context of experiments. Finally, we summarize our findings in Conclusions (Sec. IV).

II. METHODOLOGY

A. Kinetics of BZ reaction

The three-variable Oregonator model given below is based on the FKN mechanism and represents the kinetics of the BZ reaction assuming pool chemical approximation [42,43], catalyzed by traditional solution-based metal ions [55] and nanocatalysts including bare nanosheets [42] (CeNS) and NP decorated graphene-based nanocomposites (0D-2D hybrid nanocatalysts) [40,41].

$$\frac{dX}{d\tau} = k_1H^2AY - k_2HXY + k_3HAX - 2k_4X^2, \tag{1}$$

$$\frac{dY}{d\tau} = -k_1H^2AY - k_2HXY + \frac{1}{2}fk_5BZ, \tag{2}$$

$$\frac{dZ}{d\tau} = 2k_3HAX - k_5BZ. \tag{3}$$

Here, τ is the time, k_i's are the rate constants, $A = [BrO_3^-]$, $B = [\text{all oxidizable organic species}]$, $H = [H^+]$, $X = [HBrO_2]$, $Y = [Br^-]$, $Z = [\text{oxidized BZ catalyst}]$ and f is the stoichiometric coefficient [43]. To transform the dimensional form of the Oregonator model that incorporates the changes in the BZ recipe and activity of the nanocatalyst, we introduce two additional parameters, $P = \frac{H}{H_0}\frac{A}{A_0} = ha$ and $\delta = \frac{k_5}{k_{50}}\frac{B}{B_0} = \gamma b$ where $(\cdots)_0$ represent the values for the concentration of reagents and solution-based catalysts in the BZ reaction [40–42]; note that $\gamma = k_5/k_{50}$ is the activity of the nanocatalyst [42,50].

$$\frac{du}{dt} = -u^2 + Pu - fv\delta\left(\frac{u-\tilde{q}P}{u+\tilde{q}P}\right), \tag{4}$$

$$\frac{dv}{dt} = \varepsilon_0(Pu - \delta v), \tag{5}$$

TABLE I. Rate constants, catalytic activity (γ), and reference quantities for the BZ reaction system.

Rate constants [43]	Reference quantities [40,41]
$k_1 = 2\ \mathrm{M}^{-3}\ \mathrm{s}^{-1}$	$\tilde{q} = 4 \times 10^{-3}$
$k_2 = 2 \times 10^{8}\ \mathrm{M}^{-2}\ \mathrm{s}^{-1}$	$\varepsilon_0 = 8.8290 \times 10^{-4}$
$k_3 = 2 \times 10^{3}\mathrm{M}^{-2}\ \mathrm{s}^{-1}$	$H_0 = 0.9M$
$k_4 = 4 \times 10^{8}\mathrm{M}^{-1}\ \mathrm{s}^{-1}$	$A_0 = 0.23M$
$k_{50} = 1.10\ \mathrm{s}^{-1}$	$B_0 = 0.31M$
Activity (γ) of BZ catalysts	
Identifier [40–42]	Values [40–42]
CAN (solution-based)	1.00
Ce-GO (0D-2D hybrid)	1.57
Ce-rGO (0D-2D hybrid)	1.66
Ce-Graphene (0D-2D hybrid)	2.75
Ru-GO (0D-2D hybrid)	1.81
Ru-rGO (0D-2D hybrid)	3.63
Ru-Graphene (0D-2D hybrid)	11.81
CeNS (bare nanosheets)	4.90

where $u = X/X_0$, $v = Z/Z_0$, $X_0 = \frac{k_3 H_0 A_0}{2k_4}$, $Z_0 = \frac{(k_3 H_0 A_0)^2}{k_4 k_{50} B_0}$, $\varepsilon_0 = \frac{k_{50} B_0}{k_3 H_0 A_0}$, $\tilde{q} = \frac{2k_1 k_4}{k_2 k_3}$, and $t = (k_3 H_0 A_0)\tau$. Note that the above equations describe the BZ reaction with solution-based catalyst in the limiting case. The values of the parameters used in our analyses are given in Table I.

It is imperative to note that even though the nanocatalysts are present as a colloidal dispersion in the BZ reaction media [21,40–42], the reaction mixture is well mixed. This ensures the homogeneity of the chemical milieu and, therefore, allows the BZ nanocatalysts to be available for the reaction to occur without any diffusional effects [21,40–42]. Thus, the activity of nanocatalysts (γ) depends upon the reaction rate of the catalytic step of the BZ reaction mechanism [42,50], and is defined as the ratio of the rates of reaction with nanocatalyst (k_5) to traditional solution-based catalyst (k_{50}) [42,50].

The steady state concentrations (u_{ss}, v_{ss}) of the variables u and v are calculated by setting the left-hand side (LHS) of Eqs. (4) and (5) to zero, which leads to

$$u_{ss} = \frac{P}{2}\left[1 - f - \tilde{q} + \sqrt{f^2 + (1+\tilde{q})^2 - 2f(1-3\tilde{q})}\right], \quad (6)$$

$$v_{ss} = \frac{u_{ss}P}{\delta}. \quad (7)$$

From the above equations, we contemplate that u_{ss} is dependent only on P, whereas v_{ss} depends upon both P and δ.

B. Stability and higher order bifurcations

The stability of the BZ reaction system is determined by substituting $u \to u - u_{ss}$ and $v \to v - v_{ss}$ in Eqs. (4) and (5) and writing the Taylor series expansion, up to fifth order derivatives, around the steady states as [50,56]

$$\begin{aligned}[\dot{u}\ \ \dot{v}]^T = \dot{x} &= J_0 x + \tfrac{1}{2}J_1(x,x) + \tfrac{1}{6}J_2(x,x,x) \\ &+ \tfrac{1}{24}J_3(x,x,x,x) + \tfrac{1}{120}J_4(x,x,x,x,x) \\ &+ O(||x||)^6, \end{aligned} \quad (8)$$

where J_0, the 2×2 Jacobian matrix, consisting of first order derivatives of the right-hand side (RHS) of Eqs. (4) and (5), is given by

$$J_0 = \begin{bmatrix} P - 2u_{ss} - 2fP\delta\tilde{q}\frac{v_{ss}}{(u_{ss}+P\tilde{q})^2} & f\delta\left(\frac{P\tilde{q}-u_{ss}}{P\tilde{q}+u_{ss}}\right) \\ P\varepsilon_0 & -\delta\varepsilon_0 \end{bmatrix}. \quad (9)$$

The higher order derivatives in Eq. (8), represented by J_i ($i = 1 \cdots 4$), are given in Appendix A. The two characteristic roots (eigenvalues) of J_0 are

$$2\lambda_{1,2} = \mathrm{Tr}[J_0] \pm \sqrt{\mathrm{Tr}[J_0]^2 - 4\mathrm{Det}[J_0]}, \quad (10)$$

wherein $\mathrm{Tr}[J_0]$ and $\mathrm{Det}[J_0]$ are the trace and determinant of J_0, respectively. Equation (10) can be recast into a more convenient form, $\lambda_{1,2}(\mu) = \mu \pm \iota\omega_0(\mu)$, by defining $\mu = \mathrm{Tr}[J_0]/2$ and $\omega_0(\mu) = \sqrt{\mathrm{Det}[J_0] - \mu^2}$. The chemical oscillations in the BZ reaction system, therefore, depend upon the sign of μ provided $\mathrm{Det}[J_0] > \mu^2$. Evidently, when $\mu < 0$, the eigenvalues are complex conjugate with negative real parts and, hence, the system reaches steady states with decreasing amplitude of oscillations. On the other hand, when $\mu > 0$, oscillations with increasing amplitude are observed in the system and the steady states are unstable. At an intermediate value of $\mu = 0$, the eigenvalues are purely imaginary and the system transitions between oscillatory and nonoscillatory regimes and, therefore, becomes marginally stable; this transition is characterized by the occurrence of Hopf bifurcation (HB) [43]. Finally, under the condition $\mathrm{Det}[J_0] \leqslant \mu^2$, no oscillations in the system are observed as the eigenvalues are real. Thus, for the location of HB, we set $\mathrm{Tr}[J_0] = 0$ and $\mathrm{Det}[J_0] > 0$ in Eq. (10) to get

$$\begin{aligned}\eta_{\mathrm{HB}} &= \frac{\delta_{\mathrm{HB}}}{P_{\mathrm{HB}}} \\ &= \frac{1}{\varepsilon_0}\left[\frac{3f^2 + f(8\tilde{q} - 5S) - (1+\tilde{q})(-1-\tilde{q}+S)}{4f}\right],\end{aligned} \quad (11)$$

where $S = \sqrt{f^2 + (1+\tilde{q})^2 - 2f(1-3\tilde{q})}$. We treat η_{HB} as our bifurcation parameter to capture the effect of changes in the BZ recipe and the nanocatalytic activity on the BZ reaction dynamics. It is worth mentioning here that although the RHS of Eq. (11) is a function of f, ε_0, and $\tilde{q}$, we treat $\tilde{q}$ and ε_0 as constants (since they correspond to the values obtained from the standard recipe of the BZ reaction under isothermal conditions) and consider variation of f alone in our analysis.

To identify higher order bifurcations, we transform Eqs. (4) and (5) from (u, v) space into normal (or standard) form, written in terms of polar coordinates (r, θ) as [50,57]

$$\dot{r} = \mu r + L_1 r^3 + L_2 r^5 + O(|r|^7), \quad (12)$$

$$\dot{\theta} = \omega_0 + b_1 r^2 + b_2 r^4 + O(|r|^6), \quad (13)$$

$$L_1 = \tfrac{1}{2}\Re[\langle p, C(\bar{q}, q, q) + B(h_{20}, \bar{q}) + 2B(h_{11}, q)\rangle], \quad (14)$$

$$b_1 = \tfrac{1}{2}\Im[\langle p, C(\bar{q}, q, q) + B(h_{20}, \bar{q}) + 2B(h_{11}, q)\rangle], \quad (15)$$

$$\begin{aligned}L_2 = \tfrac{1}{12}\Re[&p, E(\bar{q}, \bar{q}, q, q, q) + D(q, q, q, h_{20}) \\ &+ 6D(\bar{q}, h_{11}, q, q) + 3D(\bar{q}, \bar{q}, h_{20}, q) + 3C(h_{12}, q, q)\end{aligned}$$

$$+ 6C(h_{11}, h_{11}, q) + 3C(h_{02}, h_{20}, q)$$
$$+ 6C(\bar{q}, h_{21}, q) + 6C(\bar{q}, h_{11}, h_{20}) + C(\bar{q}, \bar{q}, h_{30})$$
$$+ 3B(h_{22}, q) + 3B(h_{12}, h_{20}) + 6B(h_{11}, h_{21})$$
$$+ B(h_{02}, h_{30}) + 2B(\bar{q}, h_{21})], \tag{16}$$

$$b_2 = \tfrac{1}{12}\Re[\langle p, E(\bar{q}, \bar{q}, q, q, q) + D(q, q, q, h_{20})$$
$$+ 6D(\bar{q}, h_{11}, q, q) + 3D(\bar{q}, \bar{q}, h_{20}, q) + 3C(h_{12}, q, q)$$
$$+ 6C(h_{11}, h_{11}, q) + 3C(h_{02}, h_{20}, q) + 6C(\bar{q}, h_{21}, q)$$
$$+ 6C(\bar{q}, h_{11}, h_{20}) + C(\bar{q}, \bar{q}, h_{30}) + 3B(h_{22}, q)$$
$$+ 3B(h_{12}, h_{20}) + 6B(h_{11}, h_{21}) + B(h_{02}, h_{30})$$
$$+ 2B(\bar{q}, h_{21})\rangle], \tag{17}$$

where L_i and b_i are the respective ith Lyapunov and frequency coefficients, the expressions of which have been derived elsewhere [50].

In the above equations, the complex eigenvectors q (of J_0) and p (of J_0^T) are used to calculate the inner product represented by $\langle\cdots\rangle$. It is worth mentioning here that by considering the first terms on the RHS of Eqs. (12) and (13), i.e., the linear stability of the system, one can only identify the occurrence of HB based on the real (μ) and imaginary (ω_0) parts of the eigenvalues [see Eq. (10)]. Moreover, it is evident from Eq. (13) that the frequency of oscillations is independent of the amplitude in the linear limit. The inclusion of higher order terms in Eqs. (12) and (13), however, reveals a very rich nonlinear behavior of the BZ reaction system. For instance, when only the first two terms of Eq. (12) are considered, then the sign of L_1 determines whether HB is subcritical ($L_1 > 0$) or supercritical ($L_1 < 0$). This transition from subcritical to supercritical HB happens at $L_1 = 0$ through a higher order bifurcation, called Bautin bifurcation (or generalized HB). Likewise, the behavior of the BZ system around Bautin bifurcation can further be characterized through the calculation of L_2. Correspondingly, the nonlinear analysis also reveals that the frequency of oscillations [see Eq. (13)] is dependent upon its amplitude.

In general, the amplitude at the LCs is obtained by setting Eq. (12) equal to zero, which leads to

$$r_{\mathrm{LC}} = \sqrt{\frac{\pm\sqrt{L_1^2 - 4L_2\mu} - L_1}{2L_2}}. \tag{18}$$

The frequency of oscillations at the LC, on the other hand, can be calculated by substituting Eq. (18) in Eq. (13). Equation (18) reveals that for nonzero L_2, the BZ system can have two LCs, stable (SLC) or unstable (ULC), depending upon the values and signs of L_1 and μ. These two LCs merge into one semistable LC when $L_1^2 = 4L_2\mu$, and is known as the limit point of cycles (LPC).

C. Energy and power densities

In order to estimate the energy and power densities, we write the generalized Hamiltonian ($\mathcal{H}$) function as

$$\mathcal{H} = \mathcal{H}_c - K, \tag{19}$$

where $\mathcal{H}_c$ and K are the contributions from conservative and dissipative (nonconservative) mechanisms [58]. It is well known that any dynamical system is conservative [54] at the LC, i.e., when $\dot{r} = 0$, and dissipative otherwise. In the context of the BZ reaction, therefore, no energy (or power) can be harnessed from the chemical oscillations when the reaction is at the LC. To obtain the relevant expressions for each of the terms in Eq. (19), we transform Eqs. (12) and (13) from ordinary to canonical polar coordinates (alternatively known as standard action angle coordinates) to derive (see Appendix B) the expression for the Hamiltonian ($\mathcal{H}_c$) at the LC as follows:

$$\mathcal{H}_c = \frac{\omega_0 r_{\mathrm{LC}}^2}{2} + \frac{b_1 r_{\mathrm{LC}}^4}{4} + \frac{b_2 r_{\mathrm{LC}}^6}{6}. \tag{20}$$

The power characterized by $\dot{\mathcal{H}}$ is obtained by taking the total time derivative of Eq. (19) after the substitution of $\mathcal{H}_c$ and K (see Appendix B) as

$$\dot{\mathcal{H}} = \tfrac{1}{3} r\,\dot{r}(3r^2 b_1 + 4b_2)$$
$$= \tfrac{1}{3} r^2(\mu + L_1 r^2 + L_2 r^4)(3r^2 b_1 + 4b_2). \tag{21}$$

The above expression clearly shows that at the LC ($r = r_{\mathrm{LC}}$), $\dot{r} = 0$ and thus the power $\dot{\mathcal{H}}_{\mathrm{LC}} = 0$. To reiterate, $\mathcal{H}_c$ represents the energy stored in the chemical oscillations that is, thermodynamically, the total Gibbs free energy density of the BZ reaction [59,60].

III. RESULTS AND DISCUSSIONS

Figure 1 shows the variation of steady state concentrations of the oxidized catalyst (v_{ss}) and the activator (u_{ss}) with f computed using Eqs. (6) and (7) for nanocatalyzed BZ reactions of different formulations. In particular, Figs. 1(a) and 1(b) show (v_{ss}) (solid line) and (u_{ss}) (dotted line) along f for different values of h and γ, respectively. We observe from Fig. 1 that the profiles of all the curves remain similar; i.e., u_{ss} and v_{ss} curves pass through a point of inflection while exhibiting a monotonic decreasing trend as f increases.

The steady state profiles, shown in Figs. 1(a) and 1(b), can be analyzed from the mechanism of the BZ reaction at particular h and γ values. It is well known that the increase in f leads to an increase in the inhibitor concentration [39,43,61] which, in succession, lowers the values of u and v. This lowering of u–v values is reflected in the monotonically decreasing trends of u_{ss} and v_{ss}. To understand the occurrence of the point of inflection, let us examine the mechanism of the BZ reaction at very low and very high values of f. At lower f values, the inhibitor concentration is low, due to which the concentration of the activator remains high [39,43,61]. Consistent with the FKN mechanism, this high activator concentration results in even more production of the activator through autocatalysis [39,43,61] and thus establishes positive feedback. At higher f, however, the inhibitor concentration remains high enough to suppress the autocatalytic process and thus the rate of production of u and, consequently, the production of v, slows down. These asymmetric changes in the production rates with the increase in f are mathematically observed as the occurrence of the point of inflection. As far as the shifts in the u_{ss} and v_{ss} curves are concerned, the change in h and γ values have opposite effects. In Fig. 1(a), the increase in h leads to an

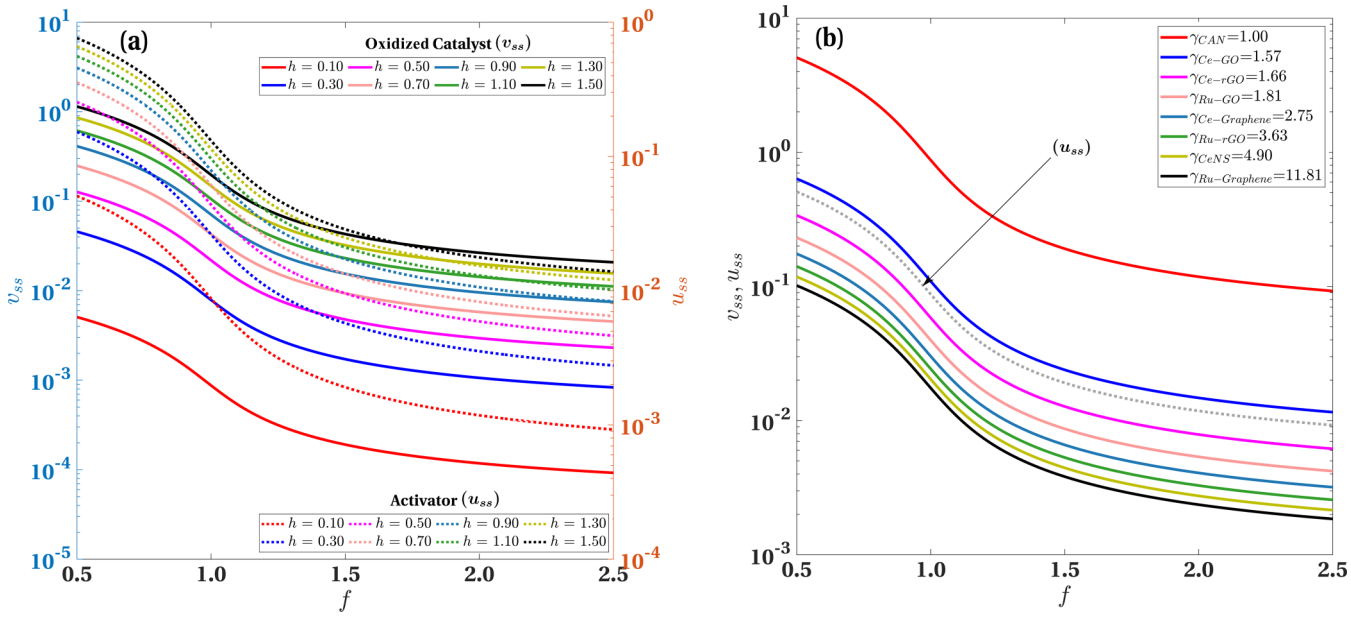

FIG. 1. The steady states profiles of oxidized catalyst (v_{ss}) and activator (u_{ss}) with stoichiometric coefficient f for different (a) h, and (b) γ values. The solid and dotted lines represent v_{ss} and u_{ss}, respectively.

overall high activator concentration, through the change in the concentrations of H species and, thus, both u_{ss} and v_{ss}, shift towards higher values. On the other hand, an increase in γ in Fig. 1(b), which signifies the increase in catalyst activity, increases the overall inhibitor concentration that ultimately translates into lower v_{ss} values [23]; the value of u_{ss}, however, remains unaffected in accordance with Eq. (6).

In Fig. 2, we explore the effect of BZ reaction formulations and nanocatalysts' activity through Hopf bifurcation (HB) curves, constructed using Eq. (11) in $\eta-f$ space; the first (L_1) and second (L_2) Lyapunov coefficients have been used to characterize HB curves as subcritical (HB^+) and supercritical (HB^-); the transition from HB^+ to HB^- occurs at Bautin bifurcation (BB). Specifically, the HB curves for different values of h and γ are shown in the respective Figs. 2(a) and 2(b) and, correspondingly, the variation of L_1 [calculated using Eq. (14)] and L_2 [calculated using Eq. (16)] for particular values of $h = 1.10$ and $\gamma = 11.81$ are captured in Figs. 2(c) and 2(d), respectively. We note that, according to Eq. (11), the variations in η also reflect the change in γ for different h, and the change in h for different γ. The area bounded by the HB curve represents the region wherein the sustained chemical oscillations in the BZ reaction are observed. Mathematically, in the region below the HB curve, $\mathrm{Tr}[J_0] > 0$ and, hence, the eigenvalues of J_0 are complex conjugate with positive real parts. Thus the HB curve demarcates the transition between the oscillatory and nonoscillatory regimes for the BZ reaction.

We witness that irrespective of the location of the HB curves in Figs. 2(a) and 2(b), the position of BB remains fixed at a particular value of f. It is evident, from Figs. 2(c) and 2(d), that at BB, the value of L_1 becomes zero, whereas L_2 remains negative. In addition, all the curves in Figs. 2(a) and 2(b) intersect the abscissa ($\eta = 0$) at the two extreme values of f, as Eq. (11) becomes quadratic in f and, therefore, independent of h and γ. In essence, Fig. 2 signifies that the increase in h and γ increases the domain of chemical oscillations for the BZ reaction. From the analyses standpoint, variations in h and γ scale the oscillatory regime, according to Eq. (11), and do not alter the dynamic characteristics of the BZ reaction system. We therefore choose $h = 1.10$ and $\gamma = 11.81$ for subsequent analyses in our manuscript. The choice of $h = 1.10$ signifies comparatively more acidic conditions, whereas $\gamma = 11.81$ indicates high activity nanocatalysts in the BZ reaction milieu. Thus the bifurcation diagrams in Fig. 2 are critical in identifying the regimes of chemical oscillations in BZ reactions, which otherwise, are quite tedious to determine via experiments and computer simulations.

In Fig. 3, we explore the details of the bifurcation diagram (of Fig. 2), for $h = 1.10$ [Fig. 3(a)] and $\gamma = 11.81$ [Fig. 3(b)], and determine dynamical characteristics [in Fig. 3(c)] exhibited by the nanocatalyzed BZ reaction system in various subregions below the HB curve. These divisions are identified through the calculations of L_1 and L_2 across the entire $\eta-f$ space using Eqs. (14) and (16), respectively. In particular, the regions $R1$, $R2$, $R3$ and $R3'$ [in Figs. 3(a) and 3(b)] separated by the respective curves HB^+, HB^-, C^0, $C^{0'}$, and the trajectories at points $W1-W4$ represented in Fig. 3(c), have been used to analyze BZ oscillations; the trajectories are determined from numerical simulations of Eqs. (4) and (5).

Let us examine the trajectories in Fig. 3(c) in the context of points $W1-W5$ of Figs. 3(a) and 3(b). It is to be noted that, along the line $W1-W5$, the value of f is fixed at 0.7 and thus u_{ss} and v_{ss} values remain unchanged [see Eqs. (6) and (7)]. When the value of η corresponds to $W1$, the BZ system is in region $R3$ wherein the eigenvalues are complex with negative real parts [see Eq. (10)]. Thus, irrespective of the initial concentrations of u and v, the chemical oscillations in the BZ reaction decay in amplitude and, ultimately,

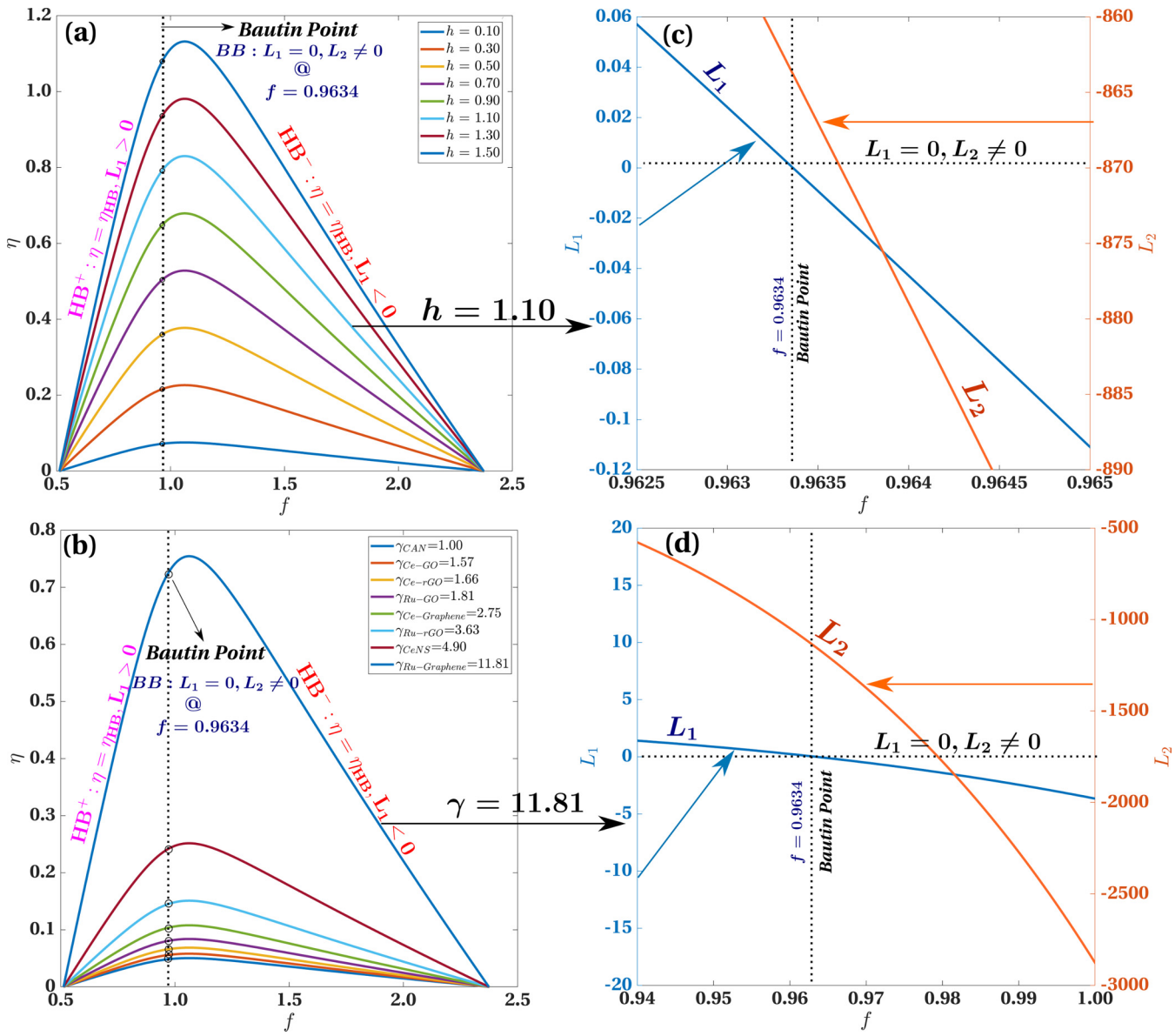

FIG. 2. The effect of BZ reaction formulations on the bifurcation diagram. The curves represent the HB line for different (a) h, and (b) γ values. The corresponding variations of L_1 and L_2 at HB for (c) $h = 1.10$, and (d) $\gamma = 11.81$ are shown.

the system approaches the steady state. Correspondingly, any trajectory for $W1$ [in Fig. 3(c)] spirals down and the steady state becomes a stable focus. Upon decrease of η to point $W2$, which lies just outside the HB^+ curve, the stable (solid circle) and unstable (dashed circle) LCs coexist, as represented in Fig. 3(c); the existence of these two LCs is evident from Eq. (18). The behavior of the BZ reaction, therefore, depends upon the initial values of u and v. When the BZ systems starts from either side of the SLC, but still remains outside the ULC, the trajectories approach the SLC [$W2$ in Fig. 3(c)]. On the contrary, when the BZ systems starts from inside the ULC, the trajectories spiral towards the steady state and, therefore, the amplitude of chemical oscillations in BZ reaction continuously decays and eventually, dies out. As we further decrease η beyond $W2$, the system crosses the HB^+ curve and reaches $W3$ in region $R2$, which is confined between the HB^+ ($L_1 > 0$) and C^0 ($L_1 = 0$) curves. As soon as the system crosses HB^+, the real part of the eigenvalues becomes positive and the steady states loses its stability. As the steady states transition from stable (at $W2$) to unstable (at $W3$), the ULC encountered at $W2$ disappears and only the SLC is left behind. Thus, any trajectory in region $R2$, irrespective of the initial conditions, approaches the SLC as shown in Fig. 3(c) (see $W3$); any further decrease of η in region $R2$ leads to an increase in the size of the SLC and, hence, the amplitudes of chemical oscillations in the BZ reaction increase.

As the system crosses C^0 and enters the region $R1$ to reach $W4$, L_1 changes its sign, from positive to negative, and a SLC of much smaller amplitude [small solid circle in Fig. 3(c)] appears. Except for the reduction in amplitude of chemical oscillations, the characteristics of the BZ reaction at $W4$ essentially remains identical to $W3$. When the system reaches $W5$ upon further reduction of η, the BZ system enters the region $R3'$ (where $L_1 > 0$) by crossing $C^{0'}$ (where

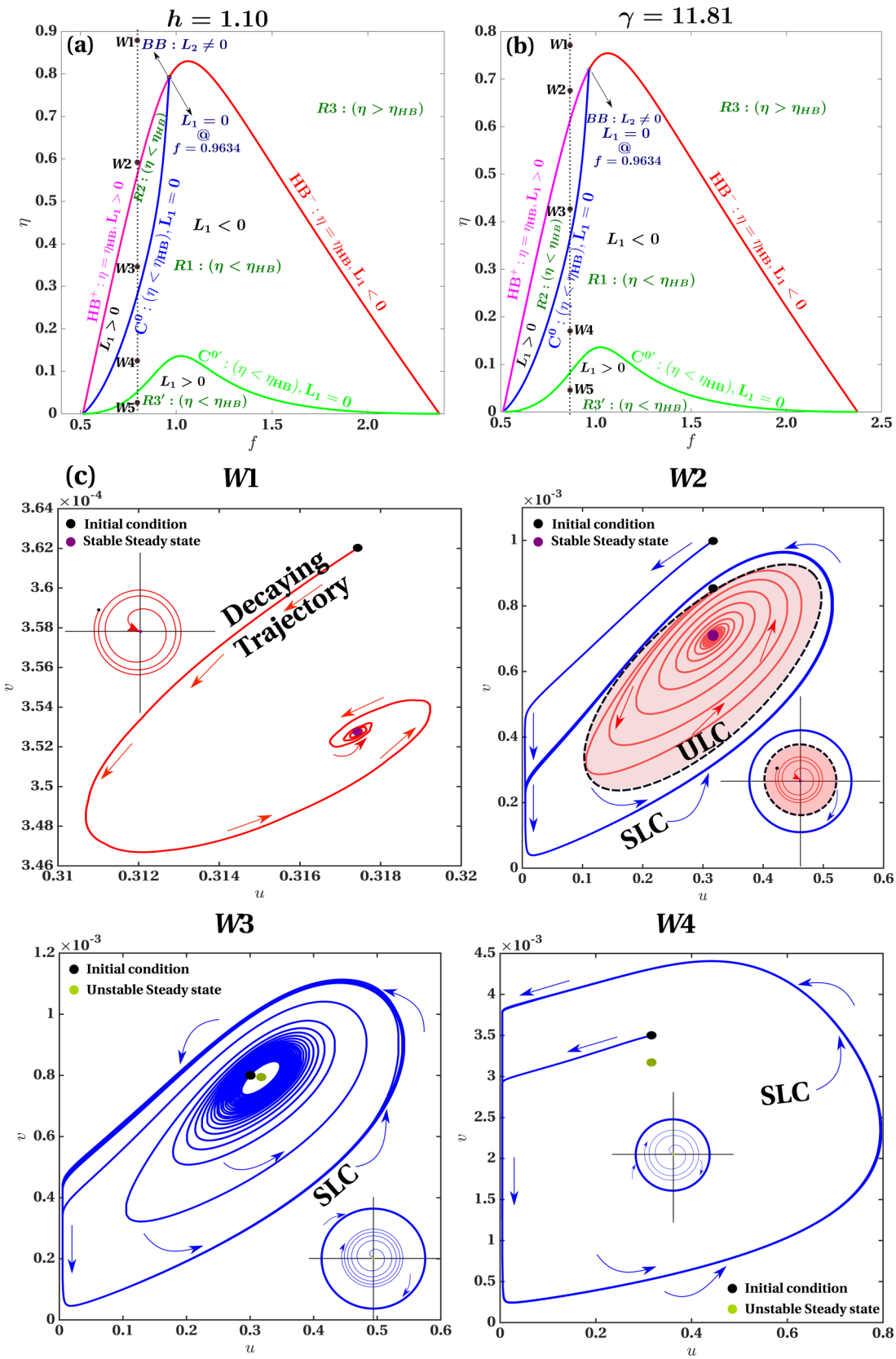

FIG. 3. The detailed bifurcation diagram with sub-regions based on the Lyapunov coefficients. The sub-regions for (a) $h = 1.10$, (b) $\gamma = 11.81$ and (c) the respective trajectories along the lines $W1 - W4$; the schematic representation of the trajectories is depicted in the inset.

$L_1 = 0$). The eigenvalues in $R3'$ become real and positive and, therefore, the SLC disappears and the unbounded trajectories (see Fig. S5 in the Supplemental Material (SM) [62]) come into existence. Consequently, as the system travels from region $R1$ to $R3'$, the BZ reaction transitions from being oscillatory to nonoscillatory (see Fig. S6 of the SM [62] for classification of regions and dynamics in terms of λ, L_1, and L_2).

In short, as we move from point $W1$ to $W5$ in Figs. 3(a) and 3(b) by reducing the value of η, no LCs exist at $W1$ and $W5$, one SLC exists at both $W3$ and $W4$, and two LCs exist at $W2$. In a physical system, the dynamical behavior of the BZ reaction described by the trajectories in Fig. 3(c) manifests as the change in the intensity of color or electrochemical potential of the BZ reaction media [40–42,63,64]. The periodic changes in these variables represent the chemical oscillations (or LC) in the BZ reaction, whereas their static values indicate steady state conditions. At unbounded trajectories ($W5$), however, both the color intensity and the electrochemical potentials continuously increase as the BZ reaction progresses.

In Fig. 4, we quantify the amplitude and frequency of chemical oscillations at the LC in different regions identified in Figs. 3(a) and 3(b) along f for two cases: first, when h is fixed and γ is varied [Figs. 4(a) and 4(c)] and second, when γ is fixed and h is varied [Figs. 4(b) and 4(d)]. The amplitudes in Figs. 4(a) and 4(b) are calculated using Eq. (18), whereas the variation of the (angular) frequencies (ω) in Figs. 4(c) and 4(d) is obtained using Eq. (13). The insets in Fig. 4 show r_{LC} and ω for particular values of γ and h, wherein the sign changes of L_1 and L_2 are depicted by shaded regions. For the sake of clarity, in the foregoing paragraphs, we first analyze amplitude variations depicted in Figs. 4(a) and 4(b) and subsequently discuss frequency variations in Figs. 4(c) and 4(d).

We witness, in Figs. 4(a) and 4(b), that irrespective of the values of γ and h, the inherent profiles of all the curves remain the same; there is one key difference, however. In Fig. 4(a), we observe that with increase in γ, r_{LC} increases, whereas in Fig. 4(b), it decreases with increase in h. In addition, r_{LC} profiles undergo many undulations with f, which are attributed to the sign changes of L_1 and L_2 (see Figs. S1 and S2 of the Supplemental Material (SM) [62]) and their relative magnitudes [computed using Eqs. (14) and (16)]. In short, r_{LC}, which represents the amplitude of chemical oscillations at the LC, is largest when γ is highest in Fig. 4(a) and h is lowest in Fig. 4(b). Moreover, the comparison between the ordinates of Figs. 4(a) and 4(b) reveals that the values of r_{LC} are about two orders of magnitude higher in Fig. 4(a).

Thus it is inferred from Figs. 4(a) and 4(b) that, in order to obtain high amplitude chemical oscillations, the scenario depicted in Fig. 4(a) is more desirable. To be specific, the increase in nanocatalyst activity must be preferred over a decrease in the acidity of the solution. From a similar line of reasoning, it is evident that finer adjustments in the amplitude of chemical oscillations can be brought about by the variations in the acidity of the solution, while the nanocatalyst activity must be used otherwise. As we have explained in Fig. 2, the interplay between activator and inhibitor concentrations with f is primarily responsible for higher values of r_{LC} at lower values of f and vice versa.

The observations in Figs. 4(c) and 4(d) are quite similar to Figs. 4(a) and 4(b); i.e., the overall profile of the curves remains the same irrespective of the parameters, γ or h. Let us analyze Figs. 4(c) and 4(d) in the context of Figs. 4(a) and 4(b). Figures 4(c) and 4(d) reveal that, as we move towards increasing values of f, the characteristics of ω change as the system enters different regions identified in Fig. 3. For instance, in Figs. 4(c) and 4(d), ω decreases for lower values of f, where the system is in the $R1$ and $R2$ regions. Likewise, when the system is in region $R3'$, where the eigenvalues are real and positive (see Fig. S3 of the SM [62]), ω is nonexistent. As soon as the system exits $R3'$ and reenters region $R1$, ω increases monotonically along f, and the change in its curvature corresponds to the sign changes in L_1 and L_2 (see Figs. S1 and S2 of the SM [62]).

The decrease and increase in ω at, respectively, lower and higher f values, are due to the variations in b_1 and b_2 computed using Eqs. (15) and (17) (see Fig. S4 of the SM [62]). The values of b_1 and b_2 remain negative with small magnitudes irrespective of the values of γ, h, and f; as a result, ω depends on amplitude (r_{LC}) only when its value is high enough. Also, since b_1 and b_2 are always negative, ω at the LC can become significantly lower than the base frequency [ω_0 in Eq. (13)] when r_{LC} is high. Thus, the undulations observed in Figs. 4(c) and 4(d) correspond to the magnitude of r_{LC} that, in turn, depends upon the sign changes in L_1 and L_2 and their relative magnitudes [see insets of Fig. 4(c) and 4(d)]. The implications of Figs. 4(c) and 4(d) for experimental investigations are similar to that of Figs. 4(a) and 4(b); i.e., variations in nanocatalyst activity must be adopted for bringing about large variations in ω, and the acidity of the solution must be tweaked to achieve its finer control.

The experimental measurements of the amplitudes of chemical oscillations (or r_{LC}) can be achieved in various ways. For instance, it has been demonstrated that the intensities of red and blue colors in the nanocatalyzed BZ reactions measured using IMP [40–42] can lead to direct determination of amplitudes. On the other hand, the determination of activator and inhibitor concentrations can also be carried out using spectrophotometric analysis wherein the absorbance of the BZ solution is measured with an UV-vis detector [63,64]. The measurements of electrochemical potential [63] in conjunction with spectrophotometric analysis, have also proved to be successful in determining the amplitudes of chemical oscillations. In these techniques, the maximum absorbance peak and the maximum deviation of electrochemical potential, which corresponds to the maximum amplitude of chemical oscillations (r_{LC}) from its reference state, are measured. As far as the frequency in a physical system is concerned, the change in ω is manifested as a fast or slow transition in the color of the BZ reaction media. Higher ω means the BZ media show faster color changes as the reaction progresses and vice versa. From a chemistry perspective, higher ω also indicates faster cyclic production and consumption of the activator (u) and inhibitor that can be measured using the techniques described above. In general, we deduce that the increase and decrease in the amplitude and frequency of chemical oscillations are in agreement with the experimental analyses reported in the literature [23,40–42,65].

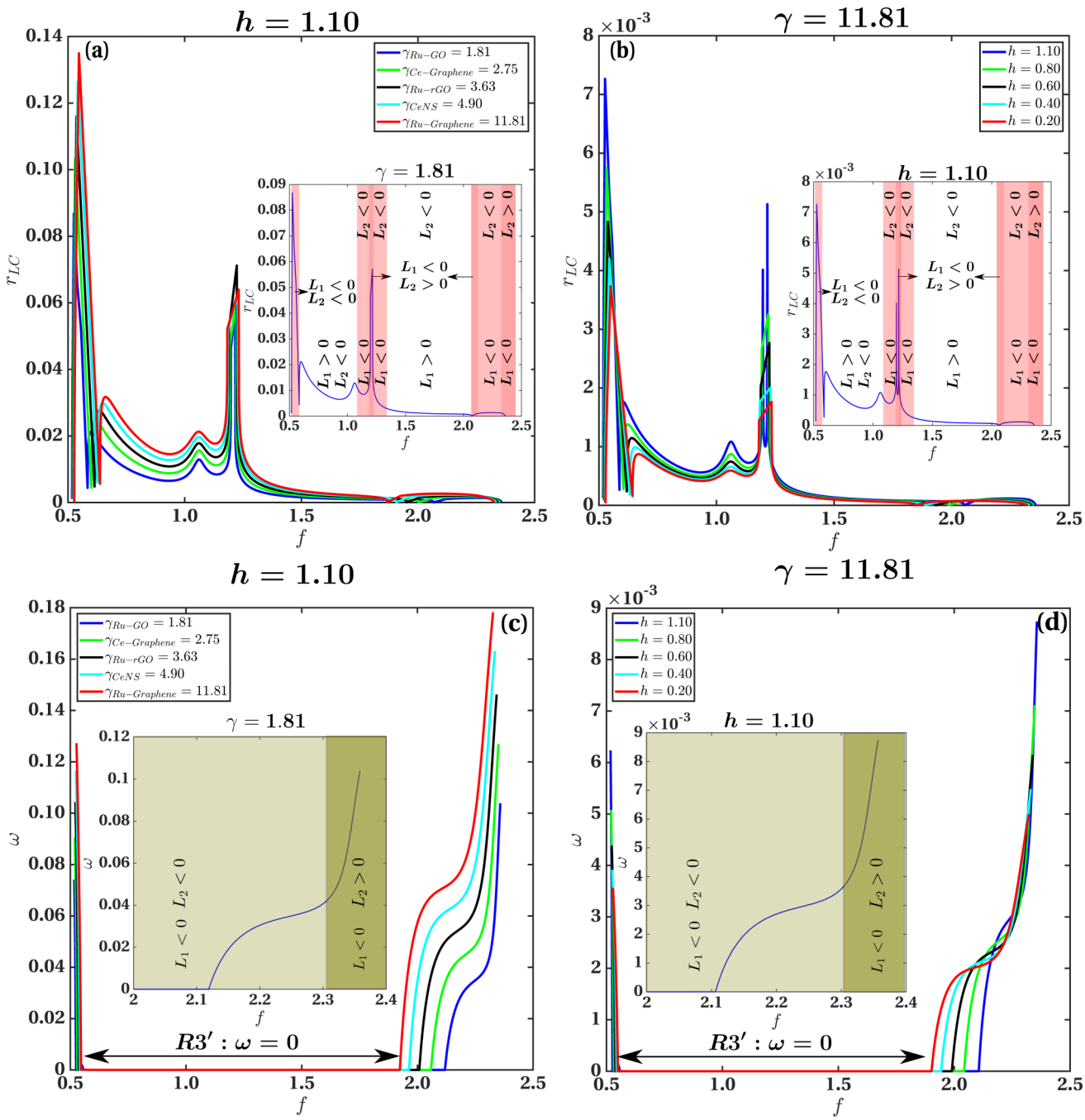

FIG. 4. The amplitude (r_{LC}) and frequency (ω) of chemical oscillations at different γ and h values with stoichiometric coefficient f. (a–b) shows the variation in r_{LC} and (c–d) shows the variation in ω with f for different values of γ when $h = 1.10$ and for different values of h when $\gamma = 11.81$. The insets in (a) and (c) shows the detailed profile for $h = 1.10$, and in (b) and (d) for $\gamma = 11.81$ that are characterized based on the signs of L_1 and L_2.

Figure 5 shows the variation of energy density ($\mathcal{H}_c$) at LCs with variation in γ and h; the insets show the magnified versions of these variations for higher values of f. In particular, Figs. 5(a) and 5(b) show the profiles of energy density ($\mathcal{H}_c$) at the LC, calculated using Eq. (20) for fixed h and γ, respectively. It is quite evident from Fig. 5 that the γ and h values do not qualitatively influence the profiles of $\mathcal{H}_c$. The insets in Figs. 5(a) and 5(b) show that as we move along the lower values of f (right to left), each $\mathcal{H}_c$ profile first increases, reaches a maximum, and then gradually drops down to zero. With the further decrease in f, the system enters the nonoscillatory regime, $R3'$, and therefore $\mathcal{H}_c$ becomes nonexistent. Moreover, just like in Fig. 3, the region $R3'$ decreases in Figs. 5(a) and 5(b) as η increases. Finally, as the systems exits $R3'$ upon lowering of f and enters the oscillatory regime $R2$, $\mathcal{H}_c$ begins to increase to even higher magnitudes and, ultimately, reaches a maximum before going to zero at $f = 0.5$. Comparison between Figs. 5(a) and 5(b) reveals that the $\mathcal{H}_c$ values for Fig. 5(a) are two orders of magnitude higher than Fig. 5(b), which is consistent with Fig. 4. Thus, tweaking

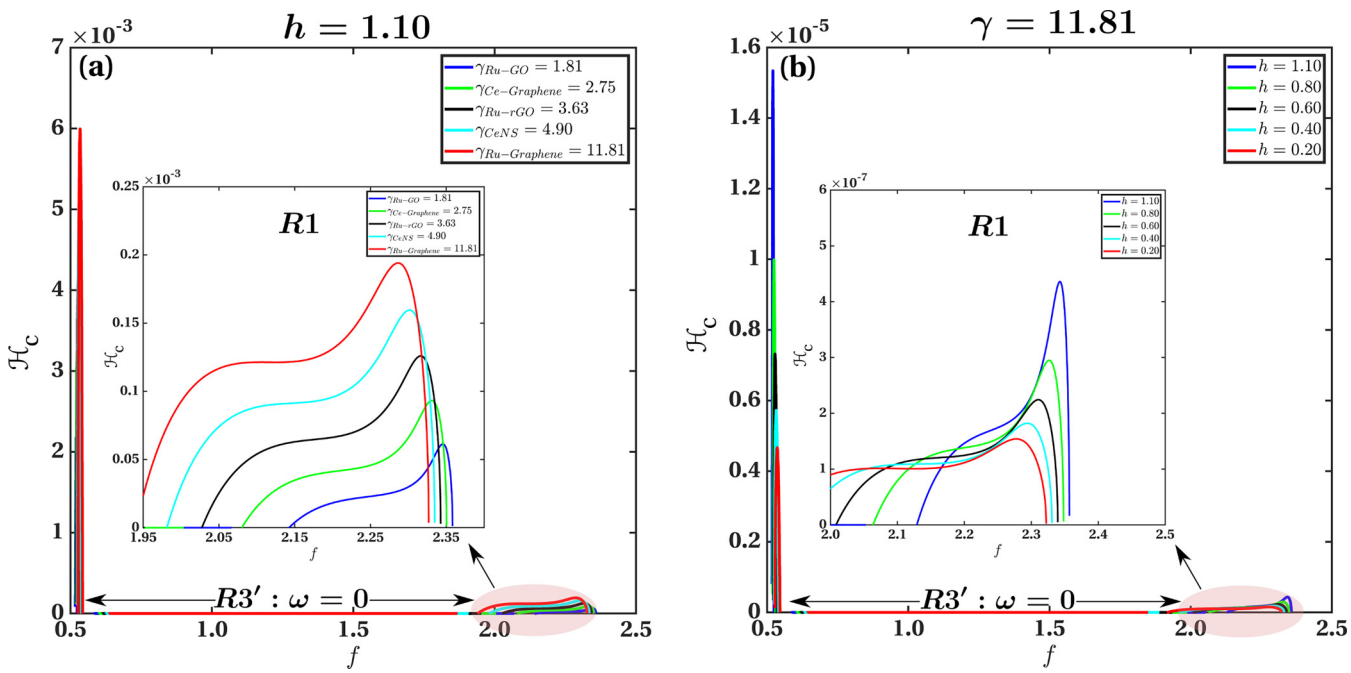

FIG. 5. The variation of energy density ($\mathcal{H}_c$) with stoichiometric coefficient f for different (a) γ when $h = 1.10$ and (b) h when $\gamma = 11.81$. The insets show the profile of $\mathcal{H}_c$ at higher f values.

the activity of the nanocatalysts, rather than the acidity of the solution, leads to large changes in the energy density of the BZ reaction at LCs.

Figure 6 shows the variation of power density ($\dot{\mathcal{H}}$) with variation in γ [Fig. 6(a)] and h [Fig. 6(b)] against the amplitude of chemical oscillations, r. It is worth mentioning here that r is different from r_{LC}, as the latter represents the amplitude at the LC. In Figs. 6(a) and 6(b), the value of r is continuously varied from zero (steady state) to r_{LC} and, therefore, all the profiles intersect abscissa at these corresponding points. In particular, in Figs. 6(a) and 6(b), the power density $\dot{\mathcal{H}}$ is obtained for a fixed f using Eq. (21) and is plotted against the amplitude (r) of chemical oscillations for different γ (when h is fixed) and h (when γ is fixed). The inset in

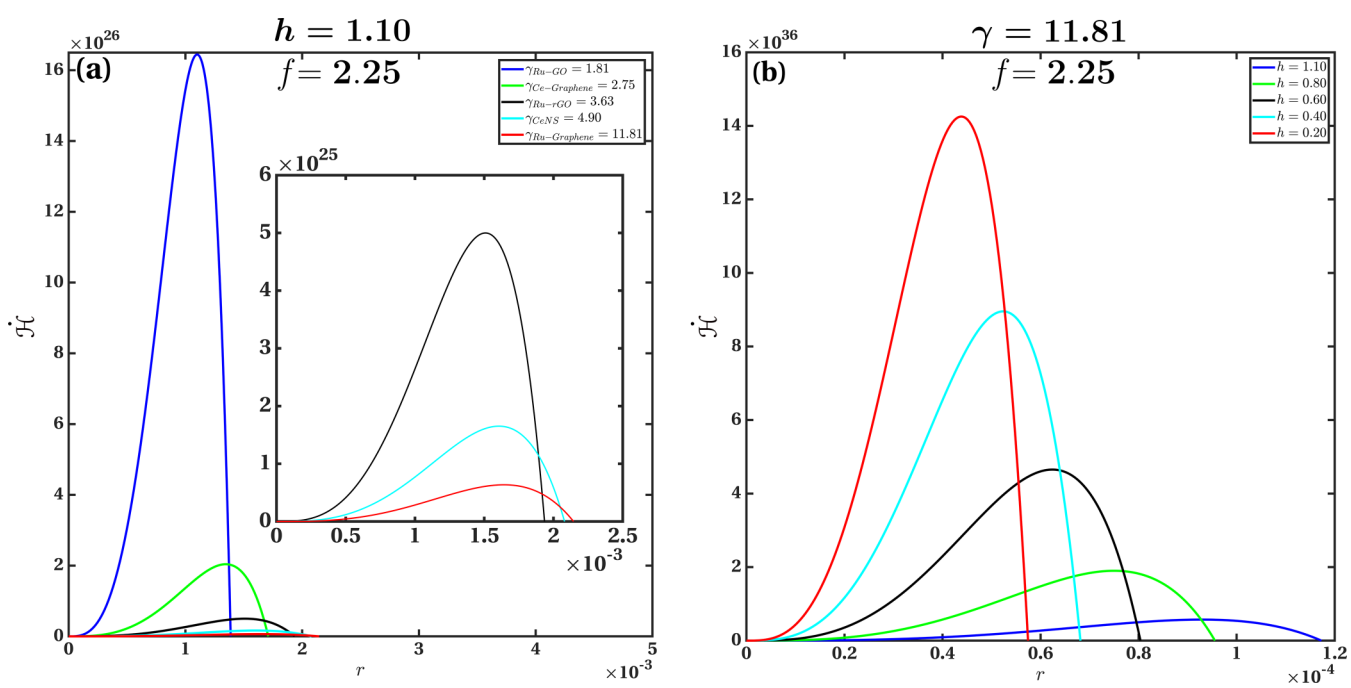

FIG. 6. The variation of power density ($\dot{\mathcal{H}}$) with stoichiometric coefficient f for different (a) γ when $h = 1.10$ and (b) h when $\gamma = 11.81$. The inset shows the enlarged profile of $\dot{\mathcal{H}}$ at higher γ.

Fig. 6(a) depicts the enlarged profile of $\dot{\mathcal{H}}$ for higher γ values. The comparison between Figs. 5(a) and 6(a) reveals that even though $\mathcal{H}_c$ is highest for Ru-Graphene, the corresponding $\dot{\mathcal{H}}$ is lowest; a similar trend is also observed for other values of γ. On the other hand, the reverse trend is observed when Figs. 5(b) and 6(b) are compared. In this case, the magnitude of $\dot{\mathcal{H}}$ is higher for Fig. 6(b) compared to Fig. 6(a). Thus, the tweaking of the acidity of the solution leads to large variations in the values of $\dot{\mathcal{H}}$.

For designing the active systems based on the BZ reaction, it becomes imperative to understand the implications of $\mathcal{H}_c$ and $\dot{\mathcal{H}}$. Mathematically, $\mathcal{H}_c$ represents the energy density in a conserved system and, therefore, no power from the BZ oscillations can be harnessed to continuously energize external systems; this is revealed from Figs. 6(a) and 6(b) wherein $\dot{\mathcal{H}} = 0$ at r_{LC}. In other words, the external systems can be continuously powered when the BZ reaction is in the nonconserved state; i.e., the BZ reaction operates between steady state and the LC (see Fig. 3: 1, $R2$, vicinity of $W2$ in $R3$). To elaborate, when the steady state is unstable and the BZ reaction exhibits the SLC ($R1$, $R2$ in Fig. 3), the oscillations can be harnessed to continuously power the external systems and, consequently, the amplitude of BZ oscillations (r) decreases, compared to its amplitude at SLC (r_{LC}), by an amount that corresponds to the power drawn by the external system. On the contrary, when the BZ reaction exhibits a stable steady state together with the ULC (Fig. 3: vicinity of $W2$ in $R3$), the chemical oscillations continuously decrease and external systems can be powered for a very short period of time. In either case, the magnitude of power generated depends on the nanocatalyst activity and acidity of the BZ reaction.

IV. CONCLUSIONS

We investigated the effect of different nanocatalysts and reaction formulations on the dynamical and energy-power characteristics of a nanocatalyzed BZ reaction using bifurcation analyses. To determine these attributes, we modified the Oregonator model and introduced parameters to account for the changes in the nanocatalyst activity and BZ recipe. We first computed the steady states and found that with increase in acidity, the reaction favors the production of activator. On the contrary, the production of inhibitor is enhanced when the nanocatalysts activity increases. We then performed linear stability analyses to trace the loci of HB and broadly identified the regimes of chemical oscillations with respect to changes in nanocatalyst activity including BZ formulations. Our calculations revealed that these oscillatory regimes radically expand when nanocatalyst activity or acidity of the solution is increased. Through nonlinear stability analyses, we then obtain a detailed bifurcation diagram by determining the nature of HB and subdividing the oscillatory regimes into various regions. To do so, we computed first and second Lyapunov coefficients at HB and observed that the location of BB remains invariant irrespective of the changes in nanocatalysts activity and BZ formulations. The calculations of Lyapunov and frequency coefficients at non-HB locations revealed the coexistence of SLC and ULC.

Next, we quantified the amplitude and frequency of chemical oscillations using Lyapunov and frequency coefficients in different regimes. We established that high nanocatalyst activity is more desirable to achieve chemical oscillations of large amplitudes and high frequencies, which is in agreement with the experimental studies. Furthermore, we formulated the Hamiltonian functions to calculate the energy and power densities of BZ oscillations. As expected, the energy density at the LC qualitatively follows similar characteristics as amplitude and frequency profiles; however, the power density follows the opposite behavior. In other words, the highest energy density corresponds to the lowest power density, and vice versa. Finally, we established that the power density becomes maximum when the amplitude is almost half the amplitude at the LC and becomes zero at the LC. We believe that the analyses and the framework developed in the paper can be extended to determine the energy harvesting potential of other nonlinear dynamical systems including active and stimuli-responsive material systems.

ACKNOWLEDGMENT

The authors acknowledge funding support from DST-SERB (Grant No. CRG/2022/002977) and IIT Gandhinagar.

APPENDIX A: HIGHER ORDER DERIVATIVES FOR J_i

We write Eqs. (4) and (5) as follows,

$$\frac{du}{dt} = M(u, v), \tag{A1}$$

$$\frac{dv}{dt} = N(u, v), \tag{A2}$$

and subsequently represent the higher order matrices J_i ($i = 1 \cdots 4$) in Eq. (8) using the above equations as

$$J_1 = \begin{bmatrix} M_{uu} & M_{vu} & M_{uv} & M_{vv} \\ N_{uu} & N_{vu} & N_{uv} & N_{vv} \end{bmatrix}_{2\times 4}, \tag{A3}$$

$$J_2 = \begin{bmatrix} M_{uuu} & M_{vuu} & M_{uvu} & M_{vvu} & M_{uuv} & M_{vuv} & M_{uvv} & M_{vvv} \\ N_{uuu} & N_{vuu} & N_{uvu} & N_{vvu} & N_{uuv} & N_{vuv} & N_{uvv} & N_{vvv} \end{bmatrix}_{2\times 8}, \tag{A4}$$

$$J_3 = \begin{bmatrix} M_{uuuu} & M_{vuuu} & M_{uvuu} & M_{vvuu} & M_{uuvu} & M_{vuvu} & M_{uvvu} & M_{vvvu} & M_{uuuv} \\ N_{uuuu} & N_{vuuu} & N_{uvuu} & N_{vvuu} & N_{uuvu} & N_{vuvu} & N_{uvvu} & N_{vvvu} & N_{uuuv} \end{bmatrix}$$
$$\cdots \begin{matrix} M_{vuuv} & M_{uvuv} & M_{vvuv} & M_{uuvv} & M_{vuvv} & M_{uvvv} & M_{vvvv} \\ N_{vuuv} & N_{uvuv} & N_{vvuv} & N_{uuvv} & N_{vuvv} & N_{uvvv} & N_{vvvv} \end{matrix}\Bigg]_{2\times 16}, \tag{A5}$$

TABLE II. Expressions for higher order derivatives.

Derivatives	Expressions
Second order	$M_{uu} = \frac{4\delta f v P q}{(u+Pq)^3} - 2, \quad M_{vu} = M_{uv} = -\frac{2Pq\delta f}{(u+Pq)^2}$
Third order	$M_{uuu} = -\frac{12\delta f v P q}{(u+Pq)^4}, \quad M_{vuu} = M_{uvu} = M_{uuv} = \frac{4\delta f P q}{(u+Pq)^3}$
Fourth order	$M_{uuuu} = \frac{48\delta f v P q}{(u+Pq)^5}, \quad M_{vuuu} = M_{uvuu} = M_{uuvu} = M_{uuuv} = -\frac{12\delta f P q}{(u+Pq)^4}$
Fifth order	$M_{5u} = -\frac{240\delta f v P q}{(u+Pq)^6}, \quad M_{vuuuu} = M_{uvuuu} = M_{uuvuu} = M_{uuuvu} = M_{uuuuv} = \frac{48\delta f P q}{(u+Pq)^5}$

$$
\begin{aligned}
J_4 = \Bigg[& M_{5u} \quad M_{vuuuu} \quad M_{uvuuu} \quad M_{vvuuu} \quad M_{uuvuu} \quad M_{vuvuu} \quad M_{uvvuu} \quad M_{vvvuu} \quad M_{uuuvu} \\
& N_{5u} \quad N_{vuuuu} \quad N_{uvuuu} \quad N_{vvuuu} \quad N_{uuvuu} \quad N_{vuvuu} \quad N_{uvvuu} \quad N_{vvvuu} \quad N_{uuuvu} \\
\cdots & M_{vuuvu} \quad M_{uvuvu} \quad M_{vvuvu} \quad M_{uuvvu} \quad M_{vuvvu} \quad M_{uvvvu} \quad M_{vvvvu} \quad M_{uuuuv} \quad M_{vuuuv} \\
\cdots & N_{vuuvu} \quad N_{uvuvu} \quad N_{vvuvu} \quad N_{uuvvu} \quad N_{vuvvu} \quad N_{uvvvu} \quad N_{vvvvu} \quad N_{uuuuv} \quad N_{vuuuv.} \\
\cdots & M_{uvuuv} \quad M_{vvuuv} \quad M_{uuvuv} \quad M_{vuvuv} \quad M_{uvvuv} \quad M_{vvvuv} \quad M_{uuuvv} \quad M_{vuuvv} \quad M_{uvuvv} \\
\cdots & N_{uvuuv} \quad N_{vvuuv} \quad N_{uuvuv} \quad N_{vuvuv} \quad N_{uvvuv} \quad N_{vvvuv} \quad N_{uuuvv} \quad N_{vuuvv} \quad N_{uvuvv} \\
\cdots & M_{vvuvv} \quad M_{uuuvv} \quad M_{vuvvv} \quad M_{uvvvv} \quad M_{5v} \\
\cdots & N_{vvuvv} \quad N_{uuuvv} \quad N_{vuvvv} \quad N_{uvvvv} \quad N_{5v} \Bigg]_{2\times 32}
\end{aligned}
\tag{A6}
$$

The mathematical expressions for the nonzero terms of J_i ($i = 1 \cdots 4$) are given in Table II.

APPENDIX B: DERIVATION OF HAMILTONIAN FUNCTIONS

To derive the Hamiltonian functions, we transform Eqs. (12) and (13) from $(r, \theta) \mapsto (R, \theta)$ [66–68] using $r = \sqrt{2R}$ as [58]

$$
\begin{aligned}
\begin{bmatrix} \dot{R} \\ \dot{\theta} \end{bmatrix} &= \begin{bmatrix} 2R\big(\mu + 2L_1 R + 4L_2 R^2\big) \\ \omega_0 + 2b_1 R + 4b_2 R^2 \end{bmatrix} \\
&= \begin{bmatrix} -\frac{\partial \mathcal{H}}{\partial \theta}\big|_{R=R_{\rm LC}} \\ \frac{\partial \mathcal{H}}{\partial R}\big|_{R=R_{\rm LC}} \end{bmatrix} + \begin{bmatrix} \frac{\partial K}{\partial \theta} \\ -\frac{\partial K}{\partial R} \end{bmatrix}.
\end{aligned}
\tag{B1}
$$

At $R = R_{\rm LC}$, the dissipative terms involving K are zero [58]; i.e.,

$$
\begin{aligned}
\begin{bmatrix} \dot{R} \\ \dot{\theta} \end{bmatrix}_{R=R_{\rm LC}} &= \begin{bmatrix} \underbrace{2R_{\rm LC}\big(\mu + 2L_1 R_{\rm LC} + 4L_2 R_{\rm LC}^2\big)}_{=0} \\ \omega_0 + 2b_1 R_{\rm LC} + 4b_2 R_{\rm LC}^2 \end{bmatrix} \\
&= \begin{bmatrix} -\frac{\partial \mathcal{H}}{\partial \theta}\big|_{R=R_{\rm LC}} \\ \frac{\partial \mathcal{H}}{\partial R}\big|_{R=R_{\rm LC}} \end{bmatrix}
\end{aligned}
\tag{B2}
$$

Substituting Eq. (B2) in Eq. (B1) and subsequently solving the $\dot{\theta}$ equation, we obtain the expression of K as

$$
\frac{\partial K}{\partial R} = 2b_1(R_{\rm LC} - R) + 4b_2\big(R_{\rm LC}^2 - R^2\big). \tag{B3}
$$

Integrating the above equation with boundary conditions $K(R) = K$ and $K(R_{\rm LC}) = 0$, we get

$$
K = -\tfrac{1}{3}(R - R_{\rm LC})^2[3b_1 + 4b_2(R + 2R_{\rm LC})]. \tag{B4}
$$

We then compute the expression for $\mathcal{H}$ by integrating $\dot{\theta}$ from the first part of Eq. (B1) as

$$
\mathcal{H} = \omega_0 R + b_1 R^2 + \frac{4b_2 R^3}{3} + C(\theta). \tag{B5}
$$

The constant $C(\theta)$ is obtained by differentiating Eq. (B5) with respect to θ as shown below:

$$
\frac{dC(\theta)}{d\theta} = \frac{\partial \mathcal{H}}{\partial \theta} = -2R(\mu + 2L_1 R + 4L_2 R^2). \tag{B6}
$$

Upon integrating above equation, we get

$$
C(\theta) = -2R(\mu + 2L_1 R + 4L_2 R^2)\theta. \tag{B7}
$$

Substituting Eq. (B7) in Eq. (B5), we obtain

$$
\mathcal{H} = \omega_0 R + b_1 R^2 + \frac{4b_2 R^3}{3} - 2R(\mu + 2L_1 R + 4L_2 R^2)\theta. \tag{B8}
$$

Taking the total derivative of the above equation with respect to time gives

$$
\dot{\mathcal{H}} = -2\dot{R}\theta(\mu + 4L_1 R + 12L_2 R^2). \tag{B9}
$$

Putting $R = R_{\rm LC}$ in Eqs. (B8) and (B9), we get

$$
\begin{aligned}
\mathcal{H}_c = {} & \omega_0 R_{\rm LC} + b_1 R_{\rm LC}^2 + \frac{4b_2 R_{\rm LC}^3}{3} \\
& - 2R_{\rm LC}\big(\mu + 2L_1 R_{\rm LC} + 4L_2 R_{\rm LC}^2\big)\theta,
\end{aligned}
\tag{B10}
$$

$$
\dot{\mathcal{H}}_c = -2\theta\big(\mu + 4L_1 R_{\rm LC} + 12L_2 R_{\rm LC}^2\big)(\dot{R}|_{R=R_{\rm LC}}). \tag{B11}
$$

Since, at the LC $\dot{R}|_{R=R_{\rm LC}} = 0$, i.e., $\mu + 2L_1 R_{\rm LC} + 4L_2 R_{\rm LC}^2 = 0$, we get the expressions for $\mathcal{H}_c$ and $\dot{\mathcal{H}}_c$ as follows:

$$
\mathcal{H}_c = \omega_0 {\rm R}_{\rm LC} + b_1 R_{\rm LC}^2 + \frac{4b_2 R_{\rm LC}^3}{3}, \tag{B12}
$$

$$
\dot{\mathcal{H}}_c = 0. \tag{B13}
$$

Using the back transformation from canonical polar to ordinary coordinates, $(R,\theta)\mapsto(r,\theta)$, using $r=\sqrt{2R}$, in Eqs. (B4), (B8), and (B12) we obtain the expressions for K, $\mathcal{H}$, and $\mathcal{H}_c$ as

$$K=-\frac{1}{12}\left(r^2-\mathrm{r}_{\mathrm{LC}}^2\right)^2\left[3b_1+2b_2\left(r^2+2r_{\mathrm{LC}}^2\right)\right], \tag{B14}$$

$$\mathcal{H}=\frac{1}{12}\Big[\Big(6\omega_0 r_{\mathrm{LC}}^2-3b_1\left(r^4-2r^2r_{\mathrm{LC}}^2\right)$$

$$-2b_2\left(r^6-3r^2r_{\mathrm{LC}}^4+r_{\mathrm{LC}}^6\right)\Big)\Big], \tag{B15}$$

$$\mathcal{H}_c=\frac{\omega_0 r_{\mathrm{LC}}^2}{2}+\frac{b_1 r_{\mathrm{LC}}^4}{4}+\frac{b_2 r_{\mathrm{LC}}^6}{6}. \tag{B16}$$

[1] L. D. Zarzar and J. Aizenberg, Stimuli-responsive chemomechanical actuation: A hybrid materials approach, Acc. Chem. Res. **47**, 530 (2014).

[2] A. Grinthal and J. Aizenberg, Adaptive all the way down: Building responsive materials from hierarchies of chemomechanical feedback, Chem. Soc. Rev. **42**, 7072 (2013).

[3] D. R. Morim, A. Meeks, A. Shastri, A. Tran, A. V. Shneidman, V. V. Yashin, F. Mahmood, A. C. Balazs, J. Aizenberg, and K. Saravanamuttu, Opto-chemo-mechanical transduction in photoresponsive gels elicits switchable self-trapped beams with remote interactions, Proc. Natl. Acad. Sci. USA **117**, 3953 (2020).

[4] Y. Yang, W. Zeng, P. Huang, X. Zeng, and L. Mei, Smart materials for drug delivery and cancer therapy, View **2**, 20200042 (2021).

[5] F. Arab Hassani *et al.*, Smart materials for smart healthcare—moving from sensors and actuators to self-sustained nanoenergy nanosystems, Smart Mater. Med. **1**, 92 (2020).

[6] R. Yoshida, Self-oscillating gels driven by the Belousov-Zhabotinsky reaction as novel smart materials, Adv. Mater. **22**, 3463 (2010).

[7] R. Yoshida, E. Kokufuta, and T. Yamaguchi, Beating polymer gels coupled with a nonlinear chemical reaction, Chaos **9**, 260 (1999).

[8] Y. Murase, S. Maeda, S. Hashimoto, and R. Yoshida, Design of a mass transport surface utilizing peristaltic motion of a self-oscillating gel, Langmuir **25**, 483 (2009).

[9] B. R. Yoshida, T. Takahashi, T. Yamaguchi, and H. Ichijo, Self-oscillating gels. Adv. Mater. **9**, 175 (1997).

[10] R. Yoshida, K. Takei, and T. Yamaguchi, Self-beating motion of gels and modulation of oscillation rhythm synchronized with organic acid, Macromolecules **36**, 1759 (2003).

[11] T. Wang *et al.*, Tactile chemomechanical transduction based on an elastic microstructured array to enhance the sensitivity of portable biosensors, Adv. Mater. **31**, 1803883 (2019).

[12] X. He *et al.*, Synthetic homeostatic materials with chemo-mechano-chemical self-regulation, Nature (London) **487**, 214 (2012).

[13] J. L. Arlett, E. B. Myers, and M. L. Roukes, Comparative advantages of mechanical biosensors, Nat. Nanotechnol. **6**, 203 (2011).

[14] J. J. Green and J. H. Elisseeff, Mimicking biological functionality with polymers for biomedical applications, Nature (London) **540**, 386 (2016).

[15] Z. Xu, T. Hueckel, W. T. M. Irvine, and S. Sacanna, Transmembrane transport in inorganic colloidal cell-mimics, Nature (London) **597**, 220 (2021).

[16] C. Gershenson, V. Trianni, J. Werfel, and H. Sayama, Self-organization and artificial life, Artif. Life **26**, 391 (2020).

[17] W. Hilber, Stimulus-active polymer actuators for next-generation microfluidic devices, Appl. Phys. A **122**, 751 (2016).

[18] T. Ohtake, H. Tanaka, T. Matsumoto, A. Ohta, and M. Kimura, Deformation of redox-active polymer gel based on polysiloxane backbone and bis(benzodithiolyl)bithienyl scaffold, Langmuir **30**, 14680 (2014).

[19] S. P. Marra, K. T. Ramesh, and A. S. Douglas, The constitutive response of active polymer gels, MRS Proc. **600**, 261 (1999).

[20] M. Rajabi, H. Baza, T. Turiv, and O. D. Lavrentovich, Directional self-locomotion of active droplets enabled by nematic environment, Nat. Phys. **17**, 260 (2021).

[21] D. J. P. Kumar, C. Borkar, and P. Dayal, Fast-moving self-propelled droplets of a nanocatalyzed Belousov–Zhabotinsky reaction, Langmuir **37**, 12586 (2021).

[22] K. V. S. Chaithanya, S. A. Shenoy, and P. Dayal, Hydrodynamics of a confined active Belousov-Zhabotinsky droplet, Phys. Rev. E **106**, 065103 (2022).

[23] S. M. Blagojević, S. R. Anić, Ž. D. Čupić, N. D. Pejić, and L. Z. Kolar-Anić, Malonic acid concentration as a control parameter in the kinetic analysis of the Belousov–Zhabotinsky reaction under batch conditions, Phys. Chem. Chem. Phys. **10**, 6658 (2008).

[24] N. Shanks, Modeling biological systems: The Belousov–Zhabotinsky reaction, Found. Chem. **3**, 33 (2001).

[25] K. S. Kiprijanov, Chaos and beauty in a beaker: The early history of the Belousov-Zhabotinsky reaction, Ann. Phys. **528**, 233 (2016).

[26] Z. Nagy-Ungvarai, J. J. Tyson, and B. Hess, Experimental study of the chemical waves in the cerium-catalyzed Belousov-Zhabotinskii reaction. 1. Velocity of trigger waves, J. Phys. Chem. **93**, 707 (1989).

[27] W. Jahnke and A. T. Winfree, Recipes for Belousov-Zhabotinsky reagents, J. Chem. Educ. **68**, 320 (1991).

[28] J. P. Keener and J. J. Tyson, Spiral waves in the Belousov-Zhabotinskii reaction, Phys. D (Amsterdam) **21**, 307 (1986).

[29] J. Zhang, Z. Chen, R. K. Kankala, S.-B. Wang, and A.-Z. Chen, Self-propelling micro-/nano-motors: Mechanisms, applications, and challenges in drug delivery, Int. J. Pharm. **596**, 120275 (2021).

[30] A. Somasundar and A. Sen, Chemically propelled nano and micromotors in the body: Quo vadis? Small **17**, 2007102 (2021).

[31] V. V. Singh and J. Wang, Nano/micromotors for security/defense applications. A review, Nanoscale **7**, 19377 (2015).

[32] H. Ceylan *et al.*, 3D-printed biodegradable microswimmer for theranostic cargo delivery and release, ACS Nano **13**, 3353 (2019).

[33] A. C. H. Tsang, E. Demir, Y. Ding, and O. S. Pak, Roads to smart artificial microswimmers, Adv. Intell. Syst. **2**, 1900137 (2020).

[34] A.-I. Bunea and R. Taboryski, Recent advances in microswimmers for biomedical applications, Micromachines **11**, 1048 (2020).

[35] T. M. Schierenbeck and M. C. Smith, Path to impact for autonomous field deployable chemical sensors: A case study of *in situ* nitrite sensors, Environ. Sci. Technol. **51**, 4755 (2017).

[36] X. He *et al.*, Autonomous chemical-sensing aerial robot for urban/suburban environmental monitoring, IEEE Syst. J. **13**, 3524 (2019).

[37] H. Zhou *et al.*, A modular approach to self-oscillating polymer systems driven by the Belousov–Zhabotinsky reaction, RSC Adv. **5**, 13555 (2015).

[38] T. J. Stockmann *et al.*, Scanning electrochemical microscopy of Belousov–Zhabotinsky reaction: How confined oscillations reveal short lived radicals and auto-catalytic species, Anal. Chem. **87**, 9621 (2015).

[39] R. J. Field and F. W. Schneider, Oscillating chemical reactions and nonlinear dynamics, J. Chem. Educ. **66**, 195 (1989).

[40] P. Kumar, D. J., S. Verma, K. Jasuja, and P. Dayal, Tuning the oscillatory dynamics of the Belousov–Zhabotinsky reaction using ruthenium nanoparticle decorated graphene, Phys. Chem. Chem. Phys. **21**, 3164 (2019).

[41] D. J. P. Kumar, K. R. Reddy, and P. Dayal, 0D-2D heterostructures as nanocatalysts for self-oscillating reactions: An investigation into chemical kinetics, Phys. Chem. Chem. Phys. **22**, 24516 (2020).

[42] V. Sharma and P. Dayal, Enhancing the kinetics of self-oscillating chemical reactions via catalytic ceria nanomats, J. Phys. Chem. C **124**, 19304 (2020).

[43] M. Mazzotti, M. Morbidelli, and G. Serravalle, Bifurcation analysis of the Oregonator model in the 3-D space bromate/malonic acid/stoichiometric coefficient, J. Phys. Chem. **99**, 4501 (1995).

[44] A. Arnéodo, F. Argoul, J. Elezgaray, and P. Richetti, Homoclinic chaos in chemical systems, Phys. D (Amsterdam) **62**, 134 (1993).

[45] G. Chen, A mathematical model for bifurcations in a Belousov–Zhabotinsky reaction, Phys. D (Amsterdam) **145**, 309 (2000).

[46] K. Sriram and S. Bernard, Complex dynamics in the Oregonator model with linear delayed feedback, Chaos **18**, 023126 (2008).

[47] R. J. Field and R. M. Noyes, A model illustrating amplification of perturbations in an excitable medium, Faraday Symp. Chem. Soc. **9**, 21 (1974).

[48] R. J. Field and R. M. Noyes, Oscillations in chemical systems. IV. Limit cycle behavior in a model of a real chemical reaction, J. Chem. Phys. **60**, 1877 (1974).

[49] R. J. Field, E. Koros, and R. M. Noyes, Oscillations in chemical systems. II. Thorough analysis of temporal oscillation in the bromate-cerium-malonic acid system, J. Am. Chem. Soc. **94**, 8649 (1972).

[50] V. Rajput and P. Dayal, Dynamical attributes of nanocatalyzed self-oscillating reactions via bifurcation analyses, J. Chem. Phys. **155**, 064902 (2021).

[51] R. J. Field, An introduction to nonlinear chemical dynamics: Oscillations, waves, patterns, and chaos (Epstein, I. R.; Pojman, J. A.), J. Chem. Educ. **77**, 450 (2000).

[52] F. Deng, J. Feng, and T. Ding, Chemoplasmonic oscillation: A chemomechanical energy transducer, ACS Appl. Mater. Interfaces **11**, 42580 (2019).

[53] D. Barragán, Essentials of kinetics and thermodynamics for understanding chemical oscillations, Found. Chem. **17**, 93 (2015).

[54] P. B. Kahn, *Nonlinear Dynamics: Exploration through Normal Forms* (Wiley, New York, 1998).

[55] J. J. Tyson, What everyone should know about the Belousov-Zhabotinsky reaction, in *Frontiers in Mathematical Biology*, Lecture Notes in Biomathematics Vol. 100, edited by S. A. Levin (Springer, Berlin, 1994), pp. 569–587.

[56] J. Sotomayor, L. F. Mello, and D. de Carvalho Braga, Lyapunov coefficients for degenerate Hopf bifurcations, arXiv:0709.3949v1 [math.DS].

[57] J. Guckenheimer and P. Holmes, *Nonlinear Oscillations, Dynamical Systems, and Bifurcations of Vector Fields*, Applied Mathematical Sciences Vol. 42 (Springer, New York, 1983).

[58] C. R. Galley, Classical mechanics of nonconservative systems, Phys. Rev. Lett. **110**, 174301 (2013).

[59] P. B. Kahn and Y. Zarmi, Weakly nonlinear oscillations: A perturbative approach, Am. J. Phys. **72**, 538 (2004).

[60] B. Leung, Novel dissipative Lagrange-Hamilton formalism for LC/van der Pol oscillator with new implication on phase noise dependency on quality factor, in *2014 IEEE 57th International Midwest Symposium on Circuits and Systems (MWSCAS)* (IEEE, New York, 2014), pp. 507–510.

[61] A. Cassani, A. Monteverde, and M. Piumetti, Belousov-Zhabotinsky type reactions: The non-linear behavior of chemical systems, J. Math. Chem. **59**, 792 (2021).

[62] See Supplemental Material at http://link.aps.org/supplemental/10.1103/PhysRevE.108.064211 for the variations of Lyapunov and frequency coefficients with the stoichiometric factor at different values of bifurcation parameter. In addition, the variations of trace, discriminant, and determinant of Jacobian matrix with the stoichiometric factor are included. The behavior of the BZ reaction at the nonoscillatory region ($R3'$) and the mathematical summary of conditions used for the classification of various regions and dynamics of nanocatalyzed BZ reaction have been included.

[63] M. A. Gracia-Nava, Probing the oscillating Belousov-Zhabotinskii reaction with micrometer-sized electrodes: The effect of C, Pt, and Au, Int. J. Electrochem. Sci. **14**, 7363 (2019).

[64] C. D. Baird, H. B. Reynolds, and M. A. Crawford, A microscale method to demonstrate the Belousov–Zhabotinskii Reaction, J. Chem. Educ. **88**, 960 (2011).

[65] N. B. Ganaie and G. M. Peerzada, Effects of manganese salts on an oscillatory chemical reaction in different acid media, Int. J. Chem. Eng. Appl. **1**, 256 (2010).

[66] V. I. Arnold, *Mathematical Methods of Classical Mechanics*, Graduate Texts in Mathematics Vol. 60 (Springer, New York, 1978).

[67] H. Goldstein, *Classical Mechanics* (Addison-Wesley, Boston, 1980).

[68] B. Greenspan and P. Holmes, Repeated resonance and homoclinic bifurcation in a periodically forced family of oscillators, SIAM J. Math. Anal. **15**, 69 (1984).